JOURNAL OF MATERIALS SCIENCE 15 (1980) 359–375

An analysis of the mechanics of solid phase extrusion of polymers

P. D. COATES,* A. G. GIBSON,† I. M. WARD
Department of Physics, The University of Leeds, Leeds, UK

An analysis is presented for the mechanics of the hydrostatic extrusion of polymers in the solid phase through a conical die. The analysis starts with the lower bound solution proposed by Hoffman and Sachs and includes the effects of strain, strain rate and pressure on the deformation behaviour. It is proposed that this involves knowledge of the tensile stress–strain–strain rate relationships for each polymer, and it is shown how such information for polyethylene and polyoxymethylene can be used to explain the observed behaviour of these materials in the solid-phase extrusion process.

List of symbols

α die cone semi-angle
β normal stress coefficient of tensile flow stress
d_0 initial diameter of billet
d_f die exit diameter
$\dot{\epsilon}$ axial strain rate (plug flow)
ϵ_{red} shear strain (redundant strain) incurred on crossing die entry or exit boundary
$\epsilon_N = \ln R_N = 2\ln (d_0/d_f)$ nominal true strain in extrusion
$\epsilon_f = \epsilon_{red} + \epsilon_N$
$L = \mu \cot \alpha$
μ normal stress coefficient of friction at die/billet interface
P experimental extrusion pressure = total work done per unit volume of material
P_F work done per unit volume against billet–die friction
P_I ideal deformation work done per unit volume of material
P_R total redundant work done per unit volume
$P_w = P - P_I$ "extra work" required to overcome friction, pressure and redundant strain effects
r_0 initial radius of billet
r_f die exit radius
r material radius at a point in the deformation zone
$R_N = (r_0/r_f)^2$ nominal extrusion ratio
$R = (r_0/r)^2$ extrusion ratio at a point in the deformation zone
$\sigma_0(\epsilon)$ axial tensile flow stress
$\sigma_f(\epsilon)$ process flow stress path, related to die strain and strain rate fields
σ_h tensile haul-off stress
σ_x, σ_y die stresses in deformation zone
τ_1, τ_2 shear yield stress of material at die entry and exit boundaries, respectively
v_x axial velocity
v_f extrudate velocity at die exit

1. Introduction

Converging dies have long been employed in metal forming processes such as extrusion and wire drawing. The former technique enables products to be manufactured with a wide variety of cross-sections, depending upon the shape of die used. Two methods of solid-phase extrusion have been developed: conventional extrusion, in which a ram is used to cause a billet of solid material to flow through the die, and hydrostatic extrusion, where the ram is replaced by a pressurized fluid. Hydrostatic extrusion has the advantage of eliminating friction between the billet and container, and

* Present address: School of Manufacturing Systems Engineering, University of Bradford.
† Present address: Department of Metallurgy and Materials Science, University of Liverpool.

0022–2461/80/020359–17$03.70/0

billet–die friction is also reduced by the presence of a film of lubricant. A summary of much of the extensive experimental work on the hydrostatic extrusion of metals has been given by Pugh [1].

Solid-state extrusion is a comparatively novel technique for forming polymers. Early work on hydrostatic extrusion included studies of linear polyethylene (LPE) by Buckley and Long [2], and polypropylene by Williams [3]. In this laboratory, hydrostatic extrusion studies have been made on several polymers, including LPE [4, 5], polyoxymethylene (POM) [6], polymethylmethacrylate [7], polycarbonate and nylon 6. The aim was to produce oriented rods of considerably larger cross-section than that conventionally attainable by drawing. Details of the extrusion of LPE and POM, and various physical property measurements on the extrudates have been presented elsewhere [4–6, 8–10]. A summary of much of our recent work on manufacture of high modulus polymers using drawing and hydrostatic extrusion is given in [11] Ch. 1. Nakayama and Kanetsuna have also investigated hydrostatic extrusion of LPE [12].

In addition to hydrostatic extrusion studies, workers in many other laboratories, notably Takayanagi and co-workers [12–17] and Porter and co-workers performed extensive investigations using the ram extrusion technique. Some of the results of the latter co-workers are surveyed in [11] Ch. 2.

With regard to the mechanics of solid-state extrusion, there has been considerable investigation for metals. Hoffman and Sachs [18] produced a lower bound analysis for flow in conical dies, and Pugh [1] and Avitzur [19] later presented upper bound analyses. For polymers, preliminary attempts at similar treatments have been made by Takayanagi and co-workers [14–17] in the case of ram extrusion, and Nakayama and Kanetsuna [12] for hydrostatic extrusion. Although these analyses attempted to deal with strain-hardening effects they did not take into account the very important effects of strain rate and pressure on the flow stress.

In this paper, an account of hydrostatic extrusion experiments on LPE and POM performed under isothermal conditions is followed by a brief description of the measurement of tensile deformation behaviour. The tensile deformation data, which are discussed in detail elsewhere [20], are then used as a basis for a new plasticity analysis of the mechanics of the extrusion process for polymers which takes into account in a comprehensive way the effects of strain, strain rate and pressure on the deformation behaviour. These latter factors are particularly significant for polymeric materials, in contrast to metals where all three can frequently be neglected. The approach outlined here is applicable in principle to any predominantly tensile solid-phase forming operation.

2. Experimental details

2.1. Materials

The materials used in this investigation were Rigidex 50 (R50) LPE ($\bar{M}_n = 6180$, $\bar{M}_w = 101\,450$) manufactured and supplied by B.P. Chemicals International Ltd, and Delrin 500 (D500) POM ($\bar{M}_n = 45\,000$, $\bar{M}_w \simeq 2\bar{M}_n$) manufactured and supplied by E. I. du Pont de Nemours Ltd.

It has been shown that there are some differences in behaviour between different grades of LPE [5, 21]. This is also true to some extent of POM [6]. However, in respect of the experimental behaviour described here, we have observed good reproducibility between different samples prepared from the same grade of polymer. Both of the starting materials were homopolymers, with crystallinities around 70%.

2.2. The extrusion process

The main variables in conical die extrusion are the nominal extrusion ratio, R_N, and the die cone semi-angle, α. The nominal extrusion ratio is defined as

$$R_N = \frac{\text{billet cross-sectional area}}{\text{die bore cross-sectional area}} = \left(\frac{d_0}{d_f}\right)^2.$$

With polymers the product often swells on leaving the die, and it is useful to define the "actual", or final extrusion ratio as

$$R_A = \frac{\text{billet cross-sectional area}}{\text{final product cross-sectional area}}.$$

R_N is the correct measure of deformation for process analysis, but for characterization of the products, R_A is more appropriate. In the present series of experiments the amount of die swell was fairly small [5, 6] especially for LPE.

Cylindrical billets were machined to the required diameter, with a conical nose of the same semi-angle as the die, to provide an initial seal in the die. A die semi-angle, α, of 15° was adopted for all the experiments described here. The effect of die semi-angle on the extrusion pressure has also been investigated and will be reported in a future publication.

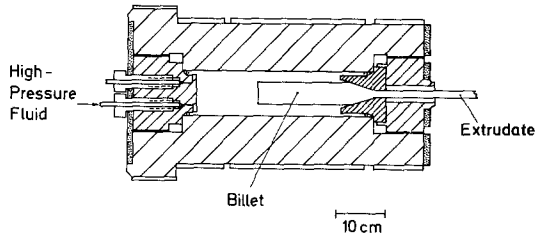

Figure 1 Apparatus used for hydrostatic extrusion.

Fig. 1 shows the apparatus employed for extrusion. The vessel can hold billets up to 75 mm diameter, for extrusion through a variety of dies. Conical dies with exit bore diameters ranging from 1.8 to 25.4 mm have been used, but the data used in this analysis are for small bore dies (1.8 and 2.5 mm) only, where it has been shown [5, 22] that for the extrusion velocities used here extrusion is approximately isothermal, the heat of deformation being conducted away by the tooling. The pressure transmitting fluid was castor oil, and the extrusion pressure was measured by an Astra Corp. pressure transducer. Heating was provided by four separately controlled band heaters, which enabled the temperature at all points along the vessel bore to be controlled within ± 1° C. After some preliminary work, extrusion temperatures of 100 and 164° C were adopted for R50 LPE and D500 POM, respectively.

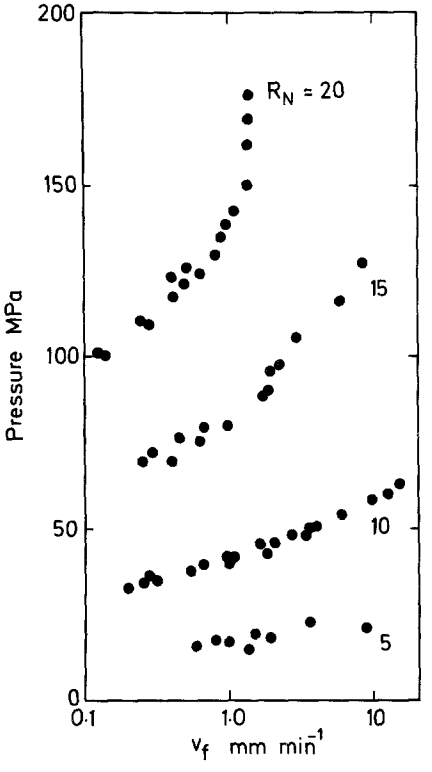

Figure 2 Rigidex 50 LPE: relationship between extrusion pressure and extrudate velocity, v_f, at 100° C for various nominal extrusion ratios.

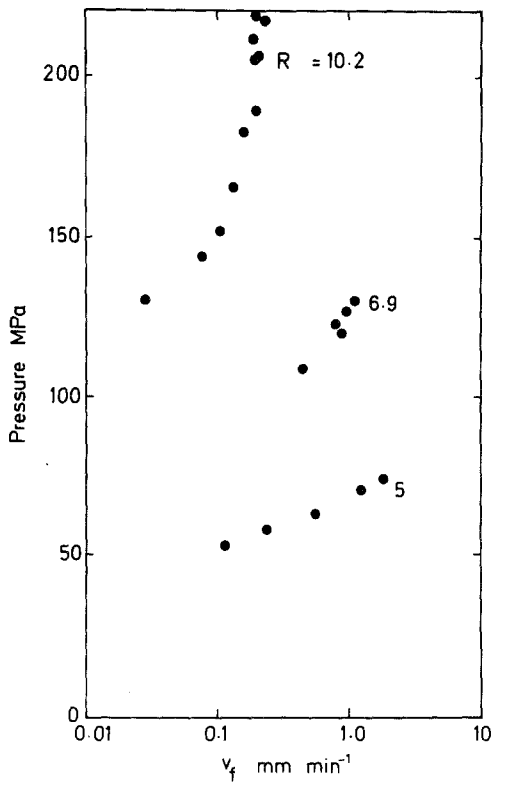

Figure 3 Delrin 500 POM: relationship between extrusion pressure and extrudate velocity v_f at 164° C for various nominal extrusion ratios.

During extrusion, a small tensile stress (≃ 1 MPa) was applied to the product using a system of weights and pulleys. This kept the extrudate straight and enabled its displacement to be measured and recorded, using the signal from a potentiometer driven by one of the pulleys. Extrusion was performed by maintaining a constant pressure within the vessel and recording the extrudate displacement. By raising the vessel pressure in small steps and recording the extrudate displacement rate at each pressure level it was possible to determine the relationship between extrusion pressure and extrusion velocity.

The pressure–velocity relationship for R50 LPE and D500 POM at a range of nominal extrusion ratios are shown in Figs. 2 and 3. The extrusion velocity shown here relates to material flow at the die bore exit, a small correction having been added to allow for die swell. The most notable feature of the behaviour for both materials is the increasing

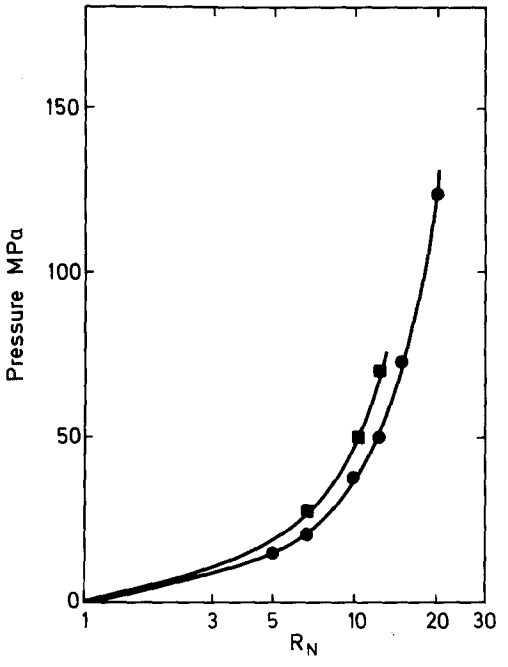

Figure 4 Rigidex 50 LPE: extrusion pressure versus nominal extrusion ratio (log scale) at constant extrudate velocities at 100° C. • $v_f = 0.5\ \text{mm min}^{-1}$, ▪ $v_f = 10\ \text{mm min}^{-1}$.

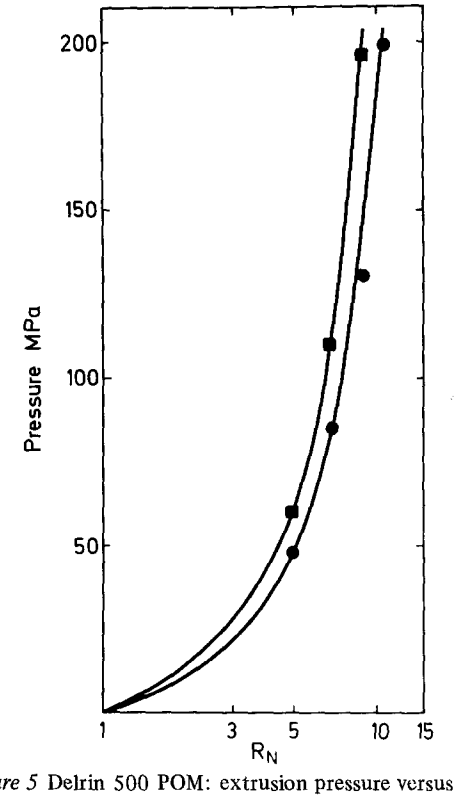

Figure 5 Delrin 500 POM: extrusion pressure versus nominal extrusion ratio (log scale) or constant extrudate velocities at 164° C. • $v_f = 0.2\ \text{mm min}^{-1}$, ▪ $v_f = 0.5\ \text{mm min}^{-1}$.

slope of the curves with increasing extrusion ratio and the pronounced upturn in pressure which occurs at higher R_N values, leading to a region where the extrusion speed becomes independent of pressure. These results for LPE and POM have been reported previously [4–6].

A further important feature of the curves in Figs. 2 and 3 is that the slope does not go to zero when they are extrapolated to low values of velocity. This casts some doubt upon the procedure suggested by Takayanagi and co-workers [14–17] and also by Nakayama and Kanetsuna [12], where a rate-independent value of the extrusion pressure is obtained by extrapolation to zero extrusion velocity. We will discuss the strain rate effects at some length in a later section and will show that a realistic understanding of the solid-state extrusion process is not possible without taking them into account.

An alternative way of presenting the data in Figs. 2 and 3 would be to show plots of pressure against R_N for constant extrudate velocity, or more significantly against $\ln R_N$ since this quantity represents the plastic strain imparted by the process. Plots of pressure versus $\ln R_N$ at constant velocity for R50 and D500 are shown in Figs. 4 and 5. Theory for non-work hardening materials predicts a linear relationship. The upward curvatures of the plots in Figs. 4 and 5 therefore suggest quite a considerable increase in the plastic flow stress with increasing deformation ratio. In both cases the pressure increases steeply with $\ln R_N$ at high extrusion ratios indicating a definite limit to the extrusion ratio attainable at a particular velocity for each material. Our analysis will show that the increase in slope with increasing $\ln R_N$ may be due not only to work hardening but also to the effect of pressure on the flow stress of the material.

Good, unflawed lengths of LPE and POM extrudates were produced throughout the range of extrusion ratios considered here, except at the highest extrusion pressures where some surface scoring was observed.

As an indication of the considerable change in properties produced by solid-state extrusion of LPE and POM, Fig. 6 shows the change in axial Young's modulus with deformation ratio. The highest value, in the case of LPE, is comparable with that of aluminium.

The purpose of the present analysis is to model the extrusion behaviour using tensile plastic deformation data for each polymer. The method of obtaining this data will now be considered.

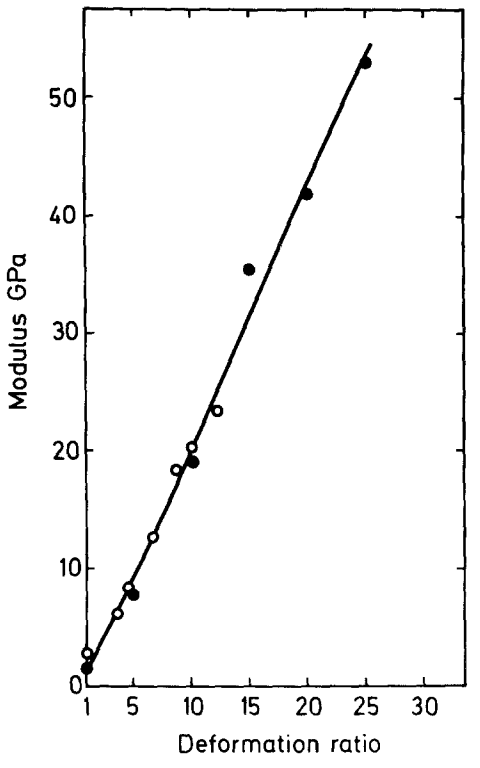

Figure 6 Relationship between axial Young's modulus (at room temperature) and actual deformation ratio. • Rigidex 50 LPE, ○ Delrin 500 POM.

2.3. Tensile deformation behaviour

2.3.1. Unique stress–strain relationships

If it can be assumed that a polymer of given initial morphology and thermal history possesses a unique relationship between the tensile flow stress, the true plastic strain and the true plastic strain rate at a fixed temperature, then true stress–strain–strain rate data collected from one type of tensile deformation test (e.g. a uniaxial tensile test) can be used to study its behaviour in other predominantly tensile deformation processes.

The existence of a unique tensile true stress–strain–strain rate relationship for the material at a given temperature implies that at a particular strain level a given tensile stress will produce a unique value of plastic strain rate. Such observations have been made [20] in drawing experiments on LPE, and also on POM, at drawing temperatures of 100 and 164° C respectively, in studies connected with the present work. For a given grade of polymer, it appears justified to assume that the strain level defines the state of the material. Supporting evidence for the validity of this assumption in the temperature range of interest comes from the agreement in flow stress–strain rate values from different types of drawing experiment, and from the unique relationship which has been observed between the axial Young's modulus and the deformation ratio for drawn LPE [21]. This relationship was not affected by the strain rate path followed in drawing at a fixed temperature [20].

Deforming a material by extrusion through a conical die is a predominantly tensile deformation process at low die angles; this will be discussed briefly later. It is therefore possible to base an analysis of the extrusion process for dies of small semi-angle upon uniaxial tensile data for each polymer at the relevant temperature, strain and strain rate. This assumption of a characteristic tensile stress–strain–strain rate relationship for the material replaces the traditional assumption of isotropic plasticity theory where the flow stress is taken as a scalar function of the accumulated "effective" strain. Before considering this analysis, a brief description of the measurement of the tensile flow stress will be given.

2.3.2. Determination of tensile flow stress

The tensile flow stress was required as a function of strain and strain rate over the region of strains and strain rates applicable to the extrusion process. This involved a wide range of deformation ratios, up to $R_N = 20$ in the case of LPE, and $R_N = 12$ in the case of POM, with plastic strain rates in the range 10^{-5} to $10^{-1}\,\text{sec}^{-1}$. It is well known that a stable neck usually forms in tensile tests on crystalline polymers. The deformation behaviour can, therefore, be divided into three regions:

(i) homogeneous deformation up to the initial formation of the neck;

(ii) inhomogeneous deformation during propagation of the neck along the sample;

(iii) homogeneous deformation after the neck has propagated along the sample.

In the region of inhomogeneous deformation it is difficult to measure the true stress as a function of both strain and strain rate because the two latter quantities are related by the geometry of the neck and, therefore, cannot be varied independently.

Three types of drawing experiment were performed corresponding to the three regions described above. All tests were performed at the same temperatures as the extrusion experiments, namely 100° C for R50 and 164° C for D500 POM. The first experiment was to determine the dependence

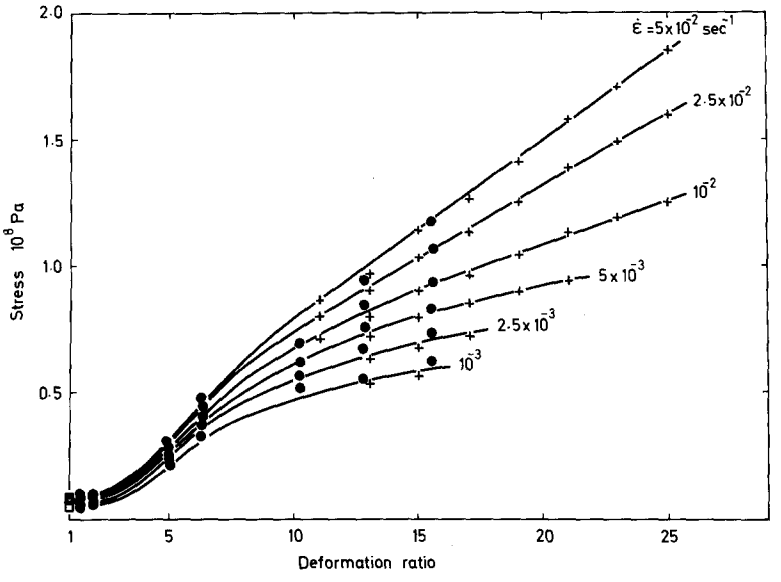

Figure 7 True stress–deformation ratio–strain rate relationships for Rigidex 50 LPE at 100° C. □ Isotropic, • extruded, + pre-drawn.

of the initial yield stress on strain rate for the isotropic polymer, by uniaxial tensile tests at constant elongation rates on an Instron tensile testing machine. At yield the specimen strain rate is assumed to be equal to the imposed machine strain rate. The second experiment was to determine the strain rate dependence of the tensile yield stress of hydrostatically extruded specimens of low and intermediate deformation ratios (from $R_n = 1.5$, up to $R_N = 15.5$ for LPE and $R_N = 9$ for POM). This experiment covered the range of deformation ratios encountered in the inhomogeneous deformation region, corresponding to the neck in a drawn specimen.

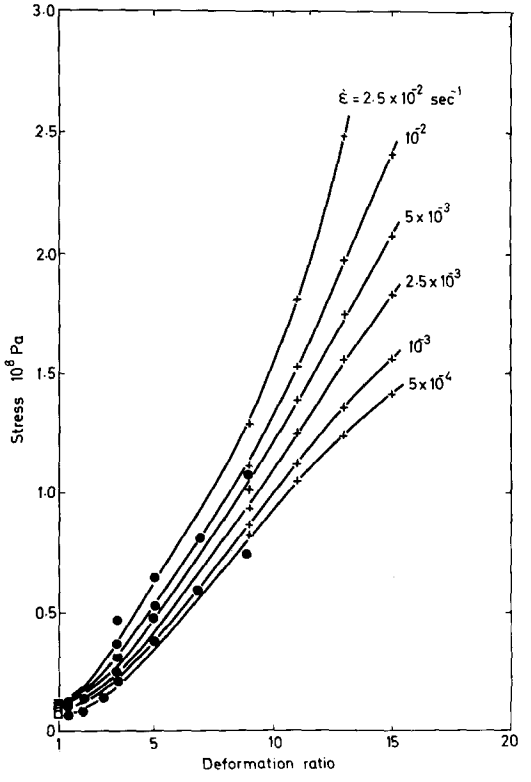

Figure 8 True stress–deformation ratio–strain rate relationships for Delrin 500 POM at 164° C. □ Isotropic, • extruded, + pre-drawn.

The third experiment involved redrawing of pre-drawn fibres of each polymer. Melt spun filaments were first drawn continuously over a heated pin (at the corresponding extrusion temperature) to deformation ratios just beyond that produced through the neck (i.e. ~ 10 for LPE and ~ 7 for POM). Samples cut from the drawn filaments were then redrawn on an Instron tensile testing machine, using a range of cross-head speeds to obtain stress–strain data at different strain rates. The fibres appeared to redraw in a macroscopically homogeneous manner so that the stress, strain and strain rate could be determined simultaneously from the specimen geometry, the drawing load and the elongation rate.

Reproducibility of the true stress data [20] was found to be within ± 5% and consistency between the results from the three types of experiment was good.

The flow stress, σ, was thus determined as a function of strain rate over a wide range of strains for R50 LPE at 100° C and D500 POM at 164° C,

and the combined results of the three drawing experiments are shown in Fig. 7 for LPE and in Fig. 8 for POM. The data in Figs. 7 and 8 could be used to represent a surface in stress–strain–strain rate space. Any predominantly tensile deformation process would then be represented by a path across that surface.

An important feature of Figs. 7 and 8 is the very marked dependence of the axial flow stress, σ, on both strain and strain rate. It is, therefore, of great importance to take account of strain and strain rate effects in considering any tensile deformation process applied to these polymers. The strain rate dependence has generally been neglected by previous workers seeking to model the extrusion behaviour of such polymers on the basis of tensile drawing data.

3. Analysis of the mechanics of the extrusion process

The relationship between extrusion pressure and the plastic stress–strain curve has been widely examined for metals where a satisfactory analysis can generally be made in terms of either the Tresca or the von Mises yield criterion. The effects of strain rate and pressure are usually small enough to be neglected. By contrast, the plastic deformation behaviour of crystalline polymers cannot be treated so simply. For the two polymers considered in this investigation, not only do we observe a high degree of strain hardening and associated mechanical anisotropy on tensile drawing, but the stress–strain relationship is strongly strain rate dependent. In addition, it is known that the yield behaviour of polymers is significantly influenced by pressure.

In the following plasticity analysis, these factors will be taken into consideration. First, it is necessary to consider the manner in which plastic flow occurs in the die.

3.1. Approaches to the problem of plastic flow in a conical die

Before describing the method of solution which we have adopted it is useful to discuss the alternative treatments available for plastic flow in conical dies: the "upper bound" and "lower bound" approaches.

3.1.1. Upper bound theory

The upper bound theorem of Prager and Hodge [23] states that "a kinematically admissible velocity field which minimizes the work done is the actual velocity field". The term *kinematically admissible* means that the velocity field must satisfy continuity requirements. Although the actual velocity field may not be known exactly, a reasonable one sufficiently close to it will give an *overestimate* of the work dissipation which is close to the true value. To find the rate of working in a plastic deformation process it is necessary to sum the various components of work within the deformation zone and over its boundaries. For conical die extrusion, therefore, the extrusion pressure is given by three components:

(i) P_I the work done within the deformation zone (per unit volume of material extruded);

(ii) P_R the "redundant" work performed at the entrance and exit of the deformation zone;

(iii) P_F the "frictional" work performed over the billet-die interface.

The extrusion pressure P is given by

$$P = P_I + P_R + P_F.$$

In his treatment, Avitzur [19] assumes that the material within the deformation zone flows radially towards the die cone apex. The deformation zone is defined at the entrance and exit by spherical boundaries. This type of velocity field predicts strain distributions in the product which are in fairly good agreement with those actually observed, and the extrusion pressures calculated from this approach agree very well with experimental values.

An important point apparent from Avitzur's solution is that the internal work term, P_I, is always very close to the "ideal work", i.e. the work which would be dissipated in a homogeneous tensile deformation without redundant strains or friction. It is possible, therefore, even at quite large die angles, to regard the flow *within* the deformation zone as purely tensile. This assumption is implicit in the other well-known upper bound solution due to Pugh [1].

3.1.2. Lower bound theory

A solution which satisfies equilibrium, but not necessarily continuity should give a lower estimate for the extrusion pressure. The best known solution of this type is the equation derived by Hoffman and Sachs [18], who considered that the deformation in the die could be treated in terms of the equilibrium of a series of thin disc-like elements perpendicular to the extrusion axis.

Solutions of Hoffman and Sachs' equation give values for the extrusion pressure which are almost

identical to the sum of the terms $P_I + P_F$ obtained from the upper bound theory. This is to be expected since, for zero friction, Hoffman and Sachs' solution reduces to the expression for ideal work, which is close to P_I, and the method used by Avitzur to calculate P_F is, in fact, based upon a particular solution of Hoffman and Sachs' equation. The predictions given by the lower bound approach of Hoffman and Sachs, therefore, differ from the upper bound solutions by an amount which is almost exactly equal to P_R, the redundant work. Indeed one of the major criticisms of Hoffman and Sachs' approach has been that it fails to take account of the effects of redundant work.

In this work, we will use a form of Hoffman and Sachs' equation in which the boundary conditions have been modified to take account of redundant work and redundant strains. It can readily be shown that for conventionally plastic materials this gives a solution which is virtually identical to the upper bound solution.

Our reasons for preferring to use a modified Hoffman and Sachs' solution rather than the more conventional upper bound approach are two-fold:

(i) Hoffman and Sachs' equation allows a greater flexibility in the type of yield criterion which can be used. This is helpful in the present case, in which a pressure-dependent criterion is required;

(ii) Hoffman and Sachs' equation permits easy calculation of the stresses within the deformation zone, whereas the upper bound approach does not.

3.2. Force balance

Following Hoffman and Sachs, consideration of the pseudo-equilibrium of forces in the axial direction on a thin parallel sided element (Fig. 9) within the deformation zone leads to

$$d\sigma_x = \left[\sigma_y(1 + \mu \cot \alpha) - \sigma_x\right]\frac{2dr}{r} \qquad (1)$$

where σ_x and σ_y are the stresses in the co-ordinate system shown in Fig. 9, and μ is the billet die friction coefficient.

Since the true strain, ϵ, at some position in the deformation zone is given by

$$\epsilon = \ln\left[\frac{r_0}{r}\right]^2$$

then

$$d\epsilon = \frac{-2dr}{r}$$

and Equation 1 can be rewritten

$$\frac{d\sigma_x}{d\epsilon} = \sigma_x - \sigma_y(1 + L), \qquad (2)$$

where $L = \mu \cot \alpha$.

In terms of extrusion ratio, R

$$\frac{d\sigma_x}{dR} = \frac{\sigma_x - \sigma_y(1 + L)}{R} \qquad (3)$$

since $\epsilon = \ln R$.

The criterion for plastic flow can be expressed as

$$\sigma_0 = \sigma_x - \sigma_y \qquad (4)$$

where σ_0 is the flow stress of the material and σ_x and σ_y are principal stresses (an assumption which is clearly permissible only for small values of α). Equation 4 could represent the yield behaviour of an isotropic material obeying either of the two common yield criteria (von Mises or Tresca) since these coincide for the case of tensile flow. Such criteria are not applicable to the present case since polymers become highly anisotropic on tensile deformation. However, in the case of uniaxial tensile deformation (i.e. the case here), the Hill criterion [24] which is a generalization of the von Mises criterion to the anisotropic situation, reduces to a form compatible with Equation 4.

Using Equation 4 to eliminate σ_y from Equation 2 gives

$$\frac{d\sigma_x}{d\epsilon} = \sigma_0(\epsilon)(1 + L) - L\sigma_x. \qquad (5)$$

In the original Hoffman and Sachs treatment the following boundary conditions are used for the solution of Equation 5:

(i) deformation zone entrance:

$$\sigma_x = -P; \quad \epsilon = 0$$

where P is the extrusion pressure,

(ii) deformation zone exit:

$$\sigma_x = 0; \quad \epsilon = \epsilon_N = \ln R_N. \qquad (6)$$

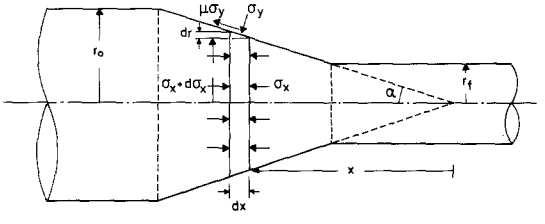

Figure 9 Hoffman and Sachs analysis; stresses on a thin parallel sided element.

It has since been established that work is done (and additional strains imparted) at the entry and exit boundaries to the deformation zone, where the material flow is forced to change direction. The average imparted strain (often called "redundant strain") at each of these boundaries is given [1, 19], for spherical deformation zone boundaries, by

$$\epsilon_{red} = \frac{1}{3}\left[\frac{\alpha}{\sin^2\alpha} - \cot\alpha\right]. \quad (7)$$

The corresponding components of "redundant work", P_1 and P_2, dissipated at the boundaries are given by

$$P_1 = \tau_1\epsilon_{red} \text{ and } P_2 = \tau_2\epsilon_{red}$$

where τ_1 and τ_2 are the appropriate shear yield stresses of the material at the die entry and exit.

To take account of these effects, the boundary conditions for solution of Equation 5 have to be changed to

$$\left.\begin{aligned} &\text{(i) } \sigma_x = -P + P_1;\ \epsilon = \epsilon_{red} \\ &\text{(ii) } \sigma_x = -P_2;\ \epsilon = \epsilon_{red} + \ln R_N. \end{aligned}\right\} \quad (8)$$

If the form of the flow stress function, $\sigma_0(\epsilon)$, is known, Equation 5 can then be solved using these boundary conditions to give the extrusion pressure and the deformation zone stresses, σ_x and σ_y.

The anisotropy which develops as a result of tensile deformation in polymers is such that although the axial flow stress $\sigma_0(\epsilon)$, increases considerably with increasing plastic strain, the yield stress for shear on planes containing the polymer chain axis changes only a little. Here it will be assumed constant and equal to the shear yield stress of the isotropic material. This approximation has little effect on the final computed pressures; the main effect of the redundant strain being to alter the *strain* boundary condition for integration of Equation 5.

3.3. Factors affecting the flow stress

3.3.1. Strain rate field

The strain rate field can be calculated to a very good approximation by assuming that only the extensional components of deformation need be considered, i.e. a planar (plug flow) velocity profile. Referring to Fig. 9, the tensile strain rate is

$$\dot{\epsilon} = \frac{dv_x}{dx} = \frac{d}{dx}\left(\frac{v_f r_f^2}{x^2\tan^2\alpha}\right) \quad (9)$$

so that

$$\dot{\epsilon} = \frac{-2v_f r_f^2}{x^3\tan^2\alpha}.$$

Rewriting in terms of deformation ratio and die exit diameter, d_f, gives

$$\dot{\epsilon} = \frac{4v_f}{d_f}\left(\frac{R}{R_N}\right)^{3/2}\tan\alpha. \quad (10)$$

v_f is the extrudate velocity at the deformation zone exit boundary and R is the instantaneous deformation ratio at a distance x from the die cone apex.

A "plug flow" velocity profile does not satisfy continuity, but gives strain rate values for small α which are in very good agreement with velocity fields which do satisfy continuity. Avitzur [19], dealing with convergent radial flow (Fig. 10), has derived the six components of plastic strain rate experienced by an infinitesimal element at some point in the deformation zone. Avitzur's work shows that deformation occurs in a predominantly tensile manner since even at comparatively large die angles the only non-negligible component of strain rate is the radial strain rate. At small α the strain rate component of convergent radial flow towards the die cone apex approximates closely to the axial strain rate, and the strain rate fields for tensile "plug flow" and convergent radial flow are almost identical. The assumption of "plug flow" implies that the axial strain rate experienced by a thin parallel sided element (shown dotted in Fig. 10) is similar to the average radial strain rate experienced by material on the spherical surface (EF in Fig. 10) passing through the centre of the element.

Equation 9 shows that the strain rate varies inversely with the cube of the distance from the die cone apex, so that close to the die exit the strain rate increases considerably. This emphasizes an important difference between the drawing pro-

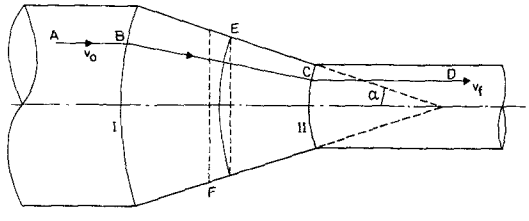

Figure 10 Convergent radial flow model. ABCD represents a typical material flow line.

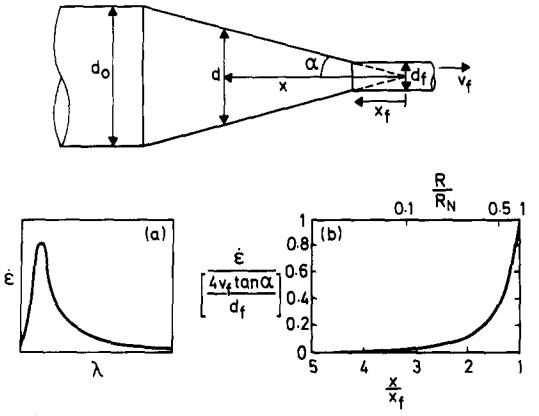

Figure 11 Variation of strain rate with deformation ratio in predominantly tensile deformation processes: (a) uniaxial tensile test (schematic); (b) hydrostatic extrusion through conical dies of small semi-angle, α.

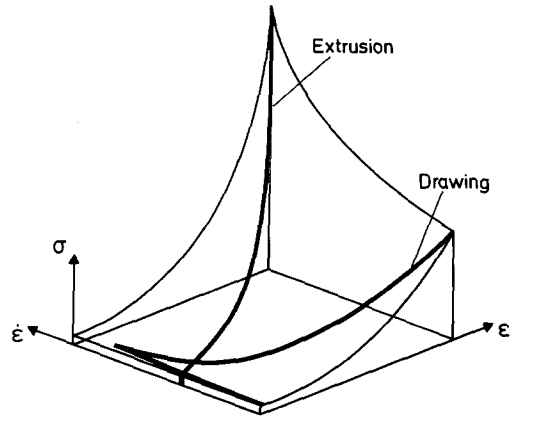

Figure 12 Schematic process stress–strain–strain rate relationships for elements of material undergoing extrusion through a conical die, and a uniaxial tensile test.

cess and the extrusion process, namely the difference in strain rate fields, as depicted in Fig. 11. In the drawing process the strain rate increases rapidly at first, corresponding to the initial neck formation, reaching a maximum in the neck region and then falling to low, decreasing values at higher draw ratios (the region of "super drawing" as it is sometimes called). In extrusion through conical dies, however, $\dot{\epsilon}$ increases steeply throughout the process. Consequently, the drawing and extrusion processes can be represented by rather different paths across the true stress–strain–strain rate surface, as shown in Fig. 12. In drawing, the material will experience lower strain rate values with increasing strain at high strains, offsetting some of the increase in flow stress caused by the increase in strain. In extrusion, increasing deformation leads to a rapid

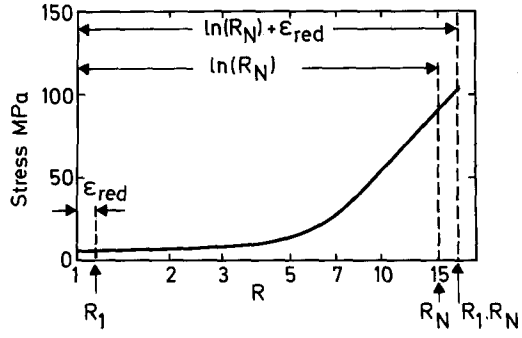

Figure 13 Effect of redundant strain, ϵ_{red}, on the boundary conditions for integration of Hoffman and Sachs' equation. Process stress–strain relationship for Rigidex 50 LPE at $R_N = 15$, $v_f = 1\ \text{mm min}^{-1}$.

increase in the flow stress due to both strain and strain rate increasing. This latter effect is likely to be particularly significant in the case of POM where the slope of the surface increases dramatically when approaching regions of high strain and strain rate.

For a particular set of process conditions (in either drawing or extrusion) an element of material will follow a particular path over the stress–strain–strain rate surface, and throughout this path ϵ and $\dot{\epsilon}$ will be related. It is therefore possible to obtain a "process stress–strain relationship', $\sigma_f(\epsilon)$. In the case of extrusion this path can be found from Equation 10 which links $\dot{\epsilon}$ and R (and hence ϵ). The values of $\sigma_f(\epsilon)$ so obtained can be used in the solution of the Hoffman and Sachs equation. The effect of the changes in the boundary conditions of integration to allow for redundant work (Section 3.2 above) is shown in Fig. 13.

3.3.2. Pressure effects

Recent work has shown that the yield behaviour of polymers can be strongly influenced by pressure [25]. The pressure dependence of isotropic polymers can be represented by considering that the critical value of the octahedral shear stress depends on the hydrostatic component of stress. For an anisotropic polymer the situation is more complicated and one approach is to start from the premise that the flow stress will be affected by the normal stress on the particular slip planes involved in the yield process, i.e. a Coulomb yield criterion. In highly oriented LPE and POM it is likely that the deformation involves slip on planes containing the chain axis. Since the chain axes become oriented in the extrusion direction at relatively low defor-

mation ratios, it is reasonable to assume that the yield behaviour will be affected by the stress σ_y normal to the extrusion direction, as well as by the resolved shear stress $\sigma_x - \sigma_y$. The normal stress effect will be assumed to be separable from the effects of strain and strain rate on the flow stress, increasing the flow stress by a factor $(1 + \beta\sigma_y)$. The normal stress coefficient β is analogous to the coefficient of friction in the Coulomb yield criterion. These assumptions lead to a modified flow criterion of the form

$$\sigma_x - \sigma_y = \sigma_f(\epsilon)(1 + \beta\sigma_y). \quad (11)$$

This form of the flow criterion produces a reasonable fit to the results of Davis and Pampillo [26] for a high molecular weight LPE in room temperature tensile tests at various applied pressures, with $\beta = -3.5\,\text{GPa}^{-1}$.

Using Equation 11 to eliminate σ_y from Equation 2 gives

$$\frac{d\sigma_x}{d\epsilon} = \sigma_x - \left[\frac{\sigma_x - \sigma_f(\epsilon)}{1 + \beta\sigma_f(\epsilon)}\right](1 + L). \quad (12)$$

This differential equation, which includes the effects of pressure, friction and the material stress–strain–strain rate behaviour was solved numerically for the boundary conditions in Equation 8 and the computed extrusion pressures were compared with experimental values. Since the two unknown factors μ and β cannot be determined independently from the present data, computation was only performed for the extreme cases:

(a) zero friction ($\mu = 0$), varying β to obtain the best fit to the results;

(b) zero pressure dependence ($\beta = 0$), varying μ to obtain the fit.

In addition, it was found instructive to evaluate P_I, the ideal work. Comparing P_I with the total observed extrusion pressure shows the magnitude of the extra work required to overcome friction and pressure effects.

4. Comparison of computed and experimental extrusion pressures

To summarize the procedures described above, calculation of the extrusion pressure, P, for a given material at a given temperature, extrusion ratio, extrudate velocity and die geometry involved three steps:

(i) computation of the strain rate field in the deformation zone,

(ii) calculation of the process stress–strain relationship $\sigma_f(\epsilon)$ from true stress–strain–strain rate data, for the computed strain rate field, making allowance for the redundant strain, ϵ_{red}, at the entrance boundary to the deformation zone;

(iii) numerical solution of the modified Hoffman and Sachs equation (Equation 12) for the appropriate boundary conditions (Equation 8).

Extrusion pressures were calculated for both R50 LPE and D500 POM for the process conditions described in Section 2.2, assuming isothermal deformation. The results for each polymer will be considered separately.

4.1. R50 LPE

The experimental relationship between the applied pressure P and $\ln R_N$ for $v_f = 1\,\text{mm min}^{-1}$ is compared in Fig. 14 with the computed curves for optimum values of μ and β. In both cases a fairly good fit can be obtained, although the friction-only case tends to produce a flatter curve than the experimental results. The optimum value of μ (assuming $\beta = 0$) was 0.03, which is in good agreement with values previously obtained for hydrostatic extrusion of metals [1] and LPE [12]. The optimum value of β was $-3.5\,\text{GPa}^{-1}$ (the minus sign resulting from the fact that compressive stresses are conventionally negative). Since the

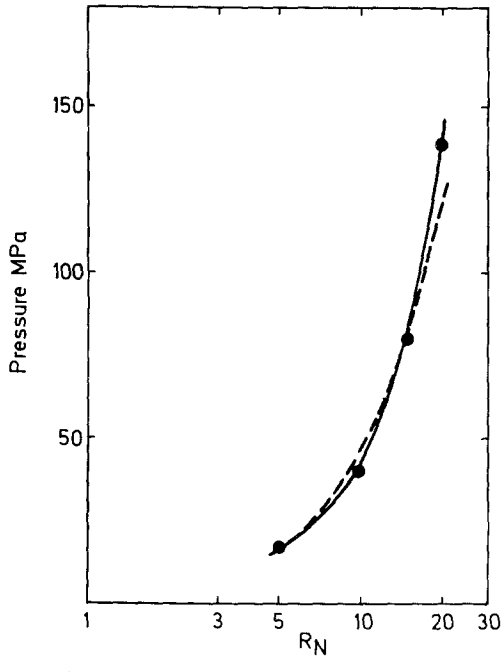

Figure 14 Rigidex 50 LPE: optimum friction and pressure-dependent fits to the experimental extrusion pressure versus $\ln R_N$ data (•) for $v_f = 1\,\text{mm min}^{-1}$. —— $\beta = -3.5\,\text{GPa}^{-1}$, – – – $\mu = 0.03$.

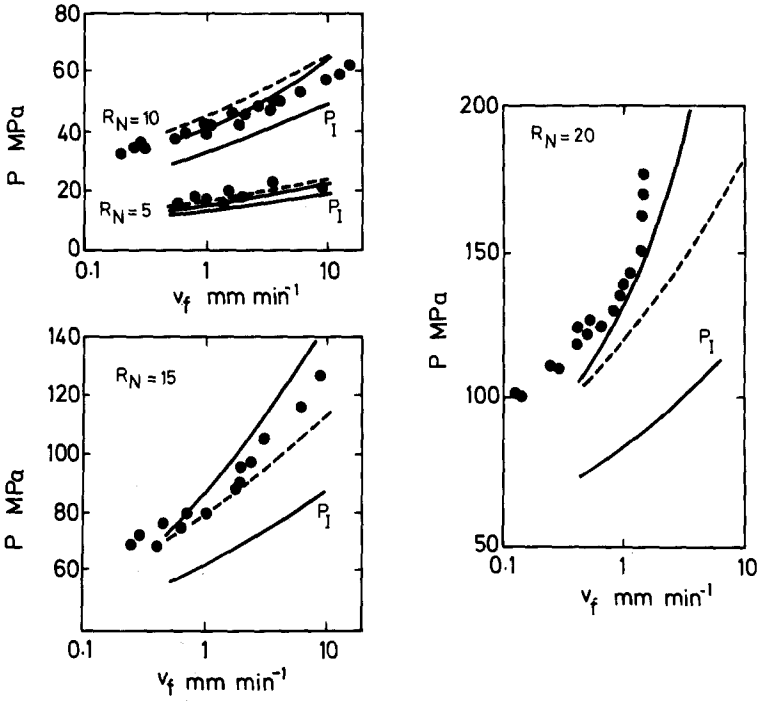

Figure 15 Rigidex 50 LPE: comparison with experimental data (•) of computed pressure–extrudate velocity relationships for optimum friction (– – –) and pressure (——) coefficients, for a range of nominal extrusion ratios.

pressure dependent fit is slightly better, this case may be nearer to the actual situation (in which both pressure and friction effects occur together).

A more stringent test of the analysis is to consider the whole range of extrusion ratios and velocities. Fig. 15 shows a comparison between the experimental pressure–velocity curves for LPE and those computed for the optimum values of μ and β determined at $v_f = 1\,\text{mm min}^{-1}$.

At low extrusion ratios ($R_N = 5$ and 10) the curves for both friction-only and pressure dependence-only fit the experimental results quite well. At higher extrusion ratios the pressure-dependent model provides a better fit to the data. Although the steep upturn of the data for $R_N = 20$ is not reproduced exactly by the pressure-dependent fit, the agreement over the whole range of v_f and R_N is quite good.

Curves showing the ideal work, P_I, have also been included in Fig. 15. The difference between the experimental pressure, P, and the ideal pressure, P_I, represents the extra work required to overcome friction and pressure effects. At low extrusion ratios this extra work is only a small fraction of the total work done per unit volume of material, but becomes increasingly significant at high extrusion ratios ($R_N > 15$), as shown in Fig. 16. In the limiting case, where v_f becomes independent of pressure, the situation is reached where an increment in extrusion pressure is balanced by the increment in extra work required to overcome the accompanying increase in flow stress and frictional work. Computed values of the total redundant work at the entry and exit boundaries, P_R, are also shown in Fig. 16, where they are seen to be quite small.

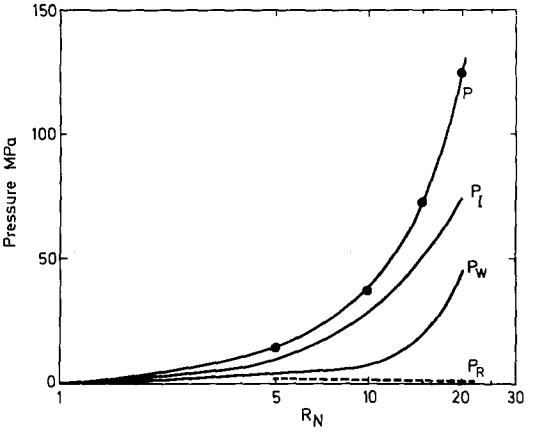

Figure 16 Rigidex 50 LPE: contributions to the extrusion pressure, P. P_I = ideal work per unit volume, P_W = extra work per unit volume ($= P - P_I$), P_R = redundant work per unit volume.

Hoffman and Sachs' analysis also allows computation of the stresses σ_x and σ_y in the deformation zone. A comparison of these die stresses is given in Fig. 17 for LPE $R_N = 20$ at two extrusion vel-

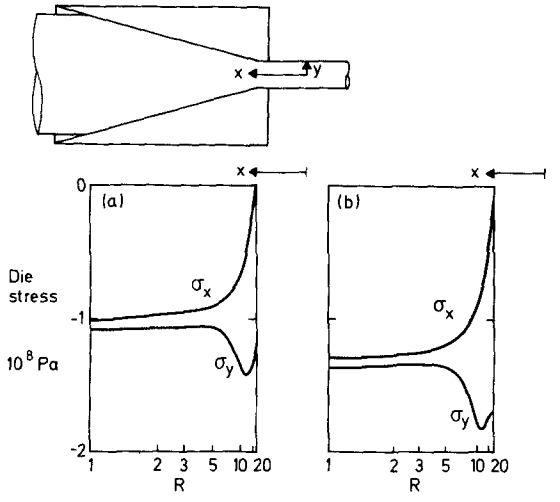

Figure 17 Rigidex 50 LPE: die stresses calculated for mm min^{-1} and (b) $v_f = 1$ mm min^{-1}. $R_N = 20$ at (a) $v_f = 0.5$

ocities, with $\beta = -3.5\,\text{GPa}^{-1}$, $\mu = 0$. As expected, σ_x falls from a value close to the extrusion pressure at the die entry boundary to a value close to zero at the die exit boundary. In the case of a non-work hardening material the curve for σ_y is parallel to that for σ_x. In the present case, however, the flow stress increases with strain, strain rate and pressure effects, so the curve for σ_y does not lie parallel to that for σ_x. In the higher extrusion velocity case, σ_y actually attains a maximum value at some point in the deformation zone which is greater than the extrusion pressure. The very high levels of σ_y could possibly account for some surface scoring observed in extrusions at high pressures.

4.2. POM

The data for POM were treated in the same manner as for LPE. The relationship between P and $\ln R_N$ is shown in Fig. 18 together with the computed curves for optimum μ and β values, at an extrudate velocity $v_f = 0.2$ mm min^{-1}. A good fit is obtained for the pressure-dependent case, the friction-only case again giving a rather flatter curve than that experimentally observed. This suggests that, as in LPE, the pressure dependent model is closer to the real situation. The optimum values of $\mu = 0.075$ and $\beta = -6.0\,\text{GPa}^{-1}$ for POM are considerably higher than those found for LPE.

The comparison of experimental and computed pressure–velocity curves for the optimum μ and β values is shown in Fig. 19. The rapid upturn in pressure at high extrusion ratios is modelled better by the pressure-dependent fit and once again the

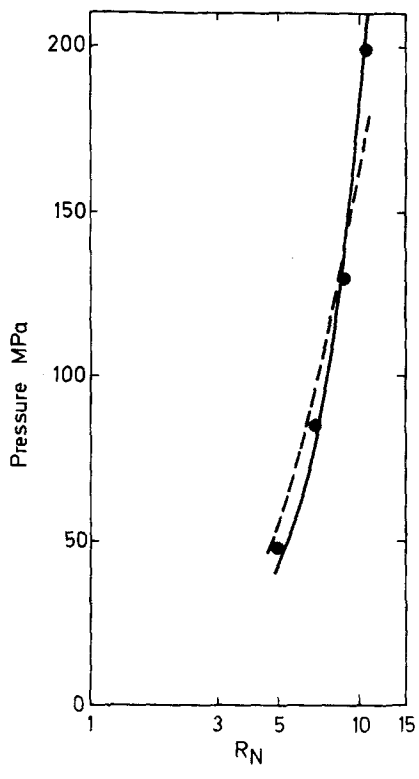

Figure 18 Delrin 500 POM: optimum friction and pressure-dependent fits to the experimental extrusion pressure versus $\ln R_N$ data (•) for $v_f = 0.2$ mm min^{-1} —— $\beta = -6$ GPa^{-1}, – – – $\mu = 0.075$.

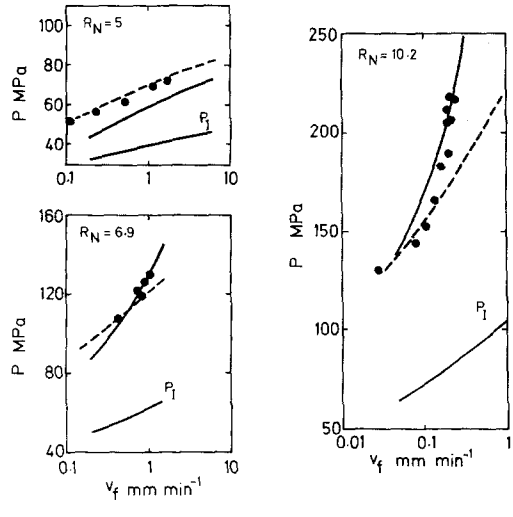

Figure 19 Delrin 500 POM: comparison of computed pressure–extrudate velocity relationships for optimum friction (– – –) and pressure (——) coefficients, for a range of nominal extrusion ratios, with experimental data (•).

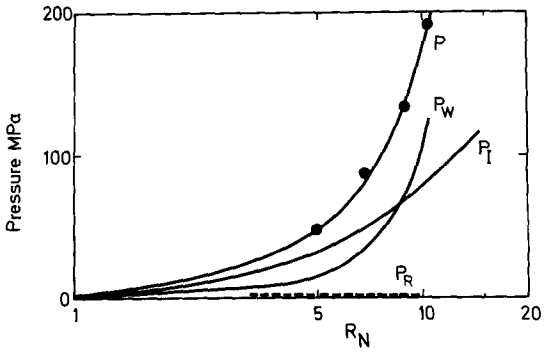

Figure 20 Delrin 500 POM: contributions to the extrusion pressure, P. P_I = ideal work done per unit volume, P_W = extra work done per unit volume ($= P - P_I$), P_R = redundant work per unit volume.

fit over the whole range of results is fairly good. Values of the ideal work of deformation are included in Fig. 19. The extra work required to overcome friction and pressure effects becomes very significant above extrusion ratios of about 6, as shown in Fig. 20. In fact, at $R_N = 9$ and above, the ideal work represents less than half of the total work done on the material. The apparently greater pressure dependence of POM probably accounts for the range of attainable extrusion ratios being more limited than the range of attainable draw ratios [6, 20]. The computed redundant work is shown in Fig. 20 and is quite small, as in the case of LPE.

5. Discussion

The basis of the present work is the application of uniaxial tensile data to an analysis of extrusion through conical dies of small semi-angles. This is done by means of the process stress–strain relationship, which takes into account the considerable differences in the strain rate fields encountered in uniaxial tensile tests and extrusion. Relationships (such as that proposed by Maruyama *et al.* [27]) which employ data from uniaxial tensile tests without taking into account the different strain rate fields in the two processes, therefore, do not give a very realistic representation of the plastic deformation behaviour. The analysis was based upon that of Hoffman and Sachs for small die angles since their treatment allows the inclusion of various forms of yield criterion, and gives very similar results to those obtained from upper bound analyses based on convergent flow.

Various means by which the extrusion process might be improved to allow higher production rates now become apparent. The expression for the axial strain field (Equation 10) indicates that one means of enhancing production rates is to design extrusion dies with a more appropriate strain rate field. For example, a constant axial strain rate die could be envisaged. This would be "trumpet shaped", having a large semi-angle α at the die entry, with α decreasing to very low values at the die exit. Such a die would produce a linear change of deformation ratio, R, with axial distance from the die entry, and the process flow stress–strain relationship would be a constant strain rate contour across the flow stress surface. Although this design would reduce the ideal work of deformation, the work done against friction would unfortunately increase greatly near the die exit.

Another feature of Equation 10 is that the strain rate field is affected by the scale of extrusion, i.e. the die exit diameter. Increasing the die exit diameter (and therefore the product diameter) should result in lowering values of $\dot{e}$ through the die. This suggests that lower extrusion pressures will be required for larger scale extrusions under otherwise fixed extrusion conditions, since deformation zone flow stress values will be lower. Alternatively, a fixed pressure level will produce a faster extrusion in the case of a larger die exit diameter. This has been observed in LPE and POM [5, 22]. As a consequence of the change in $\dot{e}$ with die exit diameter, it is best to consider results for equivalent strain rate fields (i.e. at a fixed value of v_f/d_f) when comparing the characteristics of large and small scale extrusions.

It has been observed [5] that even when large and small scale LPE extrusions are compared at equivalent strain rate fields, pressures for the former may still be lower than for the latter, as shown in Fig. 21. This is attributed to adiabatic heating of the polymer in the deformation zone causing a reduction in flow stress values. Adiabatic extrusion can clearly improve production rates but may reduce the desired improvement in properties of the extrudate. The factors determining the level of heating due to internal work dissipation are discussed at greater length by Gibson and Ward [5]. A process analysis for the adiabatic case would require knowledge of the effect of temperature on the process stress–strain relationship.

A third method of improving production rates follows from Equation 8. Application of a tensile haul-off σ_h to the product alters the die exit stress boundary condition, and can be shown [1] to

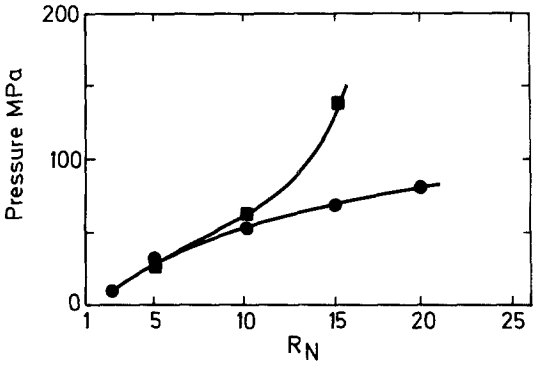

Figure 21 Rigidex 50 LPE: comparison of large and small diameter extrusions at equivalent strain rate fields, showing the effect of adiabatic heating on the pressure–nominal extrusion ratio relationship. • $d_f = 12.5$ mm, $v_f = 50$ mm min^{-1}, ▪ $d_f = 2.5$ mm, $v_f = 10$ mm min^{-1}.

result in a useful decrease in the total work done. Therefore, for a fixed extrusion pressure higher values of haul-off stress should produce faster extrusions. The practical limit to the size of σ_h is determined by the amount of draw-down which can be tolerated in the product. This process becomes drawing through the die, rather than haul-off assisted extrusion, if sufficiently high levels of σ_h are reached. It is intended to report an investigation of the effect of haul-off stress on extrusion pressure and drawing through a die in future publications.

Two adjustable parameters, μ and β, have been employed in the analysis. Maximum values obtained for the billet die friction coefficient, μ, are very low, as expected for hydrostatic extrusion and in agreement with previous measurements in the case of LPE [12]. However, it is clear that a model involving constant friction alone does not account for the observed extrusion pressure–velocity relationships. These are better modelled by the introduction of a normal stress yield criterion. Constant values of μ or β have been employed throughout this work, although it is possible that both quantities may change with strain level. In both LPE and POM, the magnitude of μ or β to produce the best fit changed slightly with R_N, but there are insufficient data to identify any trend with accuracy. It would be useful to obtain independent data on μ or β for the materials used. Attempts to determine μ under similar conditions to those encountered in the die would involve plastic deformation of the polymer and would require modelling of the somewhat uncertain lubrication conditions, and so do not appear to be practical. A more interesting (and possibly more significant) investigation would be to perform tensile tests on oriented polymer samples under pressure, to examine the validity of the normal stress criterion suggested here.

The observed difference between the computed ideal pressures and experimental pressures can be attributed mainly to the effect of pressure on the deformation behaviour of the polymer. This effect appears to limit the maximum extrusion ratio which can be attained at practical rates and to be responsible for the large upturn in the extrusion pressure–velocity relationship observed at high R_N values.

An alternative way of considering pressure effects is to propose that the large pressure–velocity upturn may be related to a pressure-induced shift in the deformation mechanism. First, it is known that the melting point [28] and mechanical relaxation peak temperatures [29] rise in a roughly linear manner with increasing pressure (by ~ 20° C per 100 MPa for LPE). Secondly, the flow stress required to produce a given strain rate in LPE is known [20] to increase rapidly with decreasing temperature. This suggests that there will be a rapid, non-linear increase in flow stress with increasing pressure at a fixed temperature.

The tensile drawing data presented briefly in Section 2.3 suggests that the drawing behaviour may be considered to be dominated by two activated processes, one of which controls the rate of plastic deformation at low stress levels and the other at high stress levels. The former process shows much smaller rate dependence than the latter and may be associated with large scale co-operative motion, possible interlamellar shear. The second process shows a greater dependence on strain and strain rate and may relate to a more localized motion with a smaller activation volume such as *c*-axis chain slip. The rapid increase in stress with increasing pressure may, therefore, be due to the high stress process. This is not normally rate controlling at 100° C at atmospheric pressure, but presumably becomes dominant with increasing pressure, as appears to be the case as the drawing temperature is lowered. This explanation suggests that it might be possible to observe a pressure upturn at lower extrusion ratios if sufficiently high pressure levels could be attained without first rapidly extruding the billet in an adiabatic manner. One way of investigating this is by the application of a back pressure to the emerging extrudate. Such

experiments have been performed on R50, and while it is not within the scope of the present paper to discuss these experiments in detail, the results indicate a steepening of the pressure–extrudate velocity curves at $R_N = 15$, and even as low as $R_N = 13$, for moderate back pressures (up to ~ 100 MPa).

A similar overall view of the pressure–velocity upturn is plausible in the case of D500 POM, although it appears that the high stress deformation process becomes significant at lower extrusion ratios than in LPE. Pressure levels are comparatively high even at low extrusion ratios due to the strong strain-hardening behaviour of POM, and the flow stress increases more rapidly with decreasing temperature than for LPE [20]. The maximum extrusion ratio which can be attained in POM ($R_N \sim 12$) is therefore much lower than the maximum useful draw ratio which can be attained ($\lambda > 20$) at a similar temperature. This contrasts with R50 LPE where comparable degrees of plastic deformation can be obtained in drawing and hydrostatic extrusion.

It is intended to discuss the effect of pressure on the plastic deformation behaviour of polymers from an activated process viewpoint elsewhere.

6. Conclusions

(1) When using flow stress data from tensile measurements to compute extrusion pressures it is necessary to take into account the differences between the strain fields in uniaxial drawing and in the extrusion process.

(2) The axial strain rate field in extrusion through dies of small semi-angle α, is related to the die geometry, so that for a given strain rate field the exit velocity is proportional to the die exit diameter, and inversely proportional to $\tan \alpha$. Knowledge of the strain rate field allows the design of a constant strain rate die, or a decreasing strain rate die.

(3) An analysis of the mechanics of the extrusion process for LPE and POM, using the Hoffman and Sachs' approach, modified to take account of (i) redundant strains at the deformation zone entry and exit boundaries, and (ii) strain rate effects, using a constant coefficient of friction, gives good agreement with experimentally observed results for low extrusion ratios. The values of μ encountered are ~ 0.03 for LPE and ~ 0.08 for POM, and are similar to the values encountered in the hydrostatic extrusion of metals. The constant friction-only model does not reproduce the rapid upturn of the pressure–velocity characteristic observed experimentally at high extrusion ratios.

(4) A modification of the analysis to include the effect of a normal stress on the tensile flow stress of the polymer considered gives reasonable agreement with experimentally observed results over the whole range of extrusion ratios and the large pressure upturn can then be reproduced. It appears that the magnitude of the normal stress coefficient β is considerably greater for POM than for LPE, ($\beta = -6.0\,\text{GPa}^{-1}$ for POM compared with $-3.5\,\text{GPa}^{-1}$ for LPE), suggesting that the effect of normal stress on the deformation behaviour of POM is greater than in the case of LPE. Our knowledge of the mechanisms involved in pressure effects at high strains is limited, and further work in this area would be valuable.

References

1. H. L. D. PUGH, "The Mechanical Behaviour of Materials under Pressure" (Elsevier, Amsterdam, London and New York, 1970).
2. A. BUCKLEY and H. A. LONG, *Polymer Eng. Sci.* 9 (1969) 115.
3. T. WILLIAMS, *J. Mater. Sci.* 8 (1973) 59.
4. A. G. GIBSON, I. M. WARD, B. N. COLE and B. PARSONS, *ibid* 9 (1974) 1193.
5. A. G. GIBSON and I. M. WARD, *J. Polymer Sci. Polymer Phys. Ed.* 16 (1978) 2015.
6. P. D. COATES and I. M. WARD, *ibid* 16 (1978) 2031.
7. N. KAHAR, R. A. DUCKETT and I. M. WARD, *Polymer* 19 (1978) 316.
8. A. G. GIBSON, D. GREIG, M. SAHOTA, I. M. WARD and C. L. CHOY, *J. Polymer Sci. Polymer Letters* 15 (1977) 183.
9. C. L. CHOY and D. GREIG, *J. Phys. C Solid State Phys.* 10 (1977) 169.
10. A. G. GIBSON, G. R. DAVIES and I. M. WARD, *Polymer* 19 (1978) 683.
11. A. CIFERRI and I. M. WARD (editors), "Ultra-High Modulus Polymers" (Applied Science Publishers, London, 1979).
12. K. NAKAYAMA and H. KANETSUNA, *Kobunshi Robunshu, Eng. Edn.* 3 (1974) 1489.
13. K. IMADA, T. YAMAMOTO, K. SHIGEMATSU and M. TAKAYANAGI, *J. Mater. Sci.* 6 (1971) 537.
14. K. NAKAMURA, K. IMADA and M. TAKAYANAGI, *Int. J. Polymeric Mater.* 2 (1972) 71.
15. K. IMADA and M. TAKAYANAGI, *ibid* 2 (1973) 89.
16. S. MARUYAMA, K. IMADA and M. TAKAYANAGI, *ibid* 2 (1973) 105.
17. *Idem*, *ibid* 2 (1973) 125.
18. O. HOFFMAN and G. SACHS, "Introduction to the Theory of Plasticity" (McGraw-Hill, New York and London, 1953).
19. B. AVITZUR, "Metalforming: Process and Analysis" (McGraw-Hill, New York and London, 1968).

20. P. D. COATES and I. M. WARD, *J. Mater. Sci.* **13** (1978) 1957.
21. G. CAPACCIO, T. A. CROMPTON and I. M. WARD, *J. Polymer Sci. Polymer Phys. Ed.* **14** (1976) 1641.
22. A. G. GIBSON, P. D. COATES and I. M. WARD, "Science and Technology of Polymer Processing", edited by Nam P. Suh and Nak-Ho Sung (MIT Press, Cambridge MA. and London, England, 1979).
23. W. PRAGER and P. G. HODGE JUN., "Theory of Perfectly Plastic Solids" (Chapman and Hall, London, 1951).
24. R. HILL, "The Mathematical Theory of Plasticity" (Oxford, Clarendon Press, 1950).
25. I. M. WARD, *J. Mater. Sci.* **6** (1971) 1397.
26. L. A. DAVIS and C. A. PAMPILLO, *J. Appl. Phys.* **42** (1971) 4659.
27. S. MARUYAMA, K. IMADA and M. TAKAYANAGI, *Int. J. Polymeric Mater.* **1** (1972) 211.
28. S. MATSUOKA, *J. Polymer Sci.* **57** (1962) 569.
29. E. JONES PARRY and D. TABOR, *J. Mater. Sci.* 8 (1973) 1510.

Received 7 March and accepted 13 June 1979.